Available online at www.sciencedirect.com
ScienceDirect
Polymer 48 (2007) 1105–1115
polymer
www.elsevier.com/locate/polymer

Formation of cylindrite structures in shear-induced crystallization of isotactic polypropylene at low shear rate

Chenggui Zhang [a,b], Haiqing Hu [a], Xiaohong Wang [a,b], Yonghua Yao [a], Xia Dong [a], Dujin Wang [a], Zhigang Wang [a], Charles C. Han [a,*]

[a] *Beijing National Laboratory for Molecular Sciences, Joint Laboratory of Polymer Science and Materials, State Key Laboratory of Polymer Physics and Chemistry, Institute of Chemistry, CAS Key Laboratory of Engineering Plastics, CAS, Beijing 100080, China*
[b] *Graduate School of Chinese Academy of Sciences, Beijing 100080, China*

Received 16 October 2006; received in revised form 11 December 2006; accepted 11 December 2006
Available online 20 December 2006

Abstract

The shear-induced crystallization behavior of isotactic polypropylene (iPP) at low shear rate and low temperature was investigated by in situ optical microscopy, time-resolved small-angle light scattering (SALS) and ex situ atomic force microscopy (AFM). Some new details and insight of the cylindrites were observed, which are important to delineate the formation mechanism of the cylindrite structures. Optical microscopic measurements showed that the core of cylindrite was formed rapidly after shear cessation, at late stage the quantity of the newly formed crystals increased and these crystals impinged into each other rapidly due to the space limitation. Measurement of the length of cylindrite core from optical microscopic observation showed that the length of cylindrite core did not change or changed very slightly with crystallization time. SALS results indicated that immediately after shear flow, the highly oriented structure emerged and the scattering intensity increased with crystallization time, and eventually the scattering patterns became circularly symmetric and the anisotropic scattering decreased, indicating the impingement of different cylindrite structures. AFM observation showed that the crystalline lamellae grew both perpendicular to and along the cylindrite core. In addition, a much wider cylindrite core was observed. Compared with the radius of gyration of a molecule, the process of shear-induced crystallization may have involved a large number of entangled molecules under a low shear rate. These evidences clearly indicate that the cylindrite core comes from the stretched bundles of the entangled network strands but not from the extended crystals of stretched single chains. A model based on the above observations has been proposed to explain the mechanism of the cylindrite developing process at low shear rate and low temperature.

Keywords: Crystallization; Shish–kebab structure; Low shear rate

1. Introduction

Usually, semicrystalline polymers are processed from melt. The final morphologies and material properties are strongly affected by the processing methods, such as injection molding, film blowing, and fiber spinning, where the molten polymers are subjected to intense shear and elongational flow [1–11]. Due to advances in the characterization techniques for polymer crystallization in recent years, flow-induced crystallization has attracted a lot of interests in many research groups, such as Keller [12–17], Hsiao [18–29], Janeschitz-Kriegl [30–32], Winter [33–36], Jeu [37,38], Monasse [39–43], Muthukumar [44–46], and many others [47–53].

Under a shear field, polymer molecules in melt are stretched in the direction of the shear field and form the extended microfibrillar structure. The shearing to the melt causes the formation of row nuclei of microfibrillar bundles, which promotes the epitaxial growth of chain-folding lamellae with the lamellar normal parallel to the long direction of row nuclei, resulting in the supermolecular morphological structure well known

* Corresponding author. Tel.: +86 10 82618089; fax: +86 10 62521519.
E-mail address: c.c.han@iccas.ac.cn (C.C. Han).

0032-3861/$ - see front matter © 2007 Elsevier Ltd. All rights reserved.
doi:10.1016/j.polymer.2006.12.025

as ''shish–kebab''. When polymer melts are sheared, polymer molecules may be oriented in the flow direction. Alignment of chain segments of polymer molecules is a natural consequence of shear. At given temperature and external shear field, the degree of orientation and the extent of alignment obviously depend on the critical entanglement molecular weight, relaxation time, helical chain conformation, etc. Hence, it is possible that, under certain experimental conditions, only partial chain strands are oriented in the flow direction, while the other chain strands, especially those near the chain ends, remain unoriented or randomly oriented with respect to the flow direction. When bundles of the oriented chain segments develop under shear, these bundles can initiate the formation of primary nuclei. Then, crystallization continues to produce the so-called ''shish–kebab'' (cylindrite) morphology.

At early stage, de Gennes [54] gave the quasi-quantitative analysis on coil–stretch transition of flexible polymer in dilute solution. He argued that the hydrodynamic interactions between chain segments vary with the degree of molecular extension. When the molecule is in a random coil conformation, only the outer segments are subjected directly to the flow field. Therefore, hydrodynamic interactions decrease as the molecule is stretched and polymer coil unwinds abruptly, when a certain critical value of the velocity gradient is reached. Keller et al. [12–17] studied shear-induced polymer crystallization in solution and stretched polymer film, and provided the first evidence of coil–stretch transition in dilute solutions under elongational flow. They thought that at a given shear rate, only molecules with high enough molecular weight can be oriented. Recently, Hsiao et al. [18–29] extended the idea of Keller. They found that during shearing, only a fraction of the chains exhibits coil–stretch transition determined by the initial chain conformation and the molecular weight, which means that only the high molecular weight polymer carries on coil–stretch transition, and the quantity of this fraction is low.

Many believe that the shish formation must be related to the mechanism of the extended chain formation in dilute polymer solution. Pennings et al. [1,2,55] studied the shish formation in dilute PE solutions under elongational flow. According to their observation, the extended chains with parallel alignment can crystallize and form micellar nuclei. Chu et al. [56,57] studied the single chain dynamics under flow in dilute polymer solutions. Their results gave the transient chain conformations, rather than the final steady-state conformations, which indeed show the fully stretched states in accordance with the predictions of coil–stretch transition. In solution crystallization, the stretched chains must exist and form shish under elongational flow, otherwise the shish–kebab structure cannot form.

Shear flow is often considered as ''weak'' flow, but for polymer melts at different stages of processing, shear affects the overall crystallization kinetics [42,43,58,59], resulting morphologies [5,11], and eventually the shish–kebab structures in the polymer matrix [5]. Most research groups have concentrated on the high shear rate flow [18,21,22,33], because it is generally believed that the low shear rate (shear rate $< 1\ s^{-1}$) cannot produce the shish–kebab structure due to the realism that chains cannot be pulled out from the network and from extended shish crystals at low shear rate. In our previous work [53], the shear-induced crystallization of iPP under low shear rate at 140 °C was reported by using in situ optical microscopy. In this article, we deeply studied the formation of shish–kebab-like cylindrite structures of iPP under low shear rate at low temperature (140 °C) by optical microscope, SALS and ex-AFM. The process of the cylindrite growth was studied by in situ optical microscopy and time-resolved SALS. By utilizing AFM, we also investigated the microstructure of cylindrite structure especially the chain bundles along the shish-like core to help to understand the formation of the cylindrites. According to the results, we have found that the mechanism of shear-induced crystallization under low shear rate at low temperature (140 °C) may be different from those reported at high shear rate and high temperature (165 °C). At high temperature the shish-like core may come from the partially stretched polymer chains, however, at low temperature the shish-like core may be formed from the deformed entangled network. The work could provide better understanding of the morphology of the cylindrite structures, and also help to delineate the formation mechanism of these shish–kebab-like cylindrites.

2. Experimental section

2.1. Materials

The iPP homopolymer was provided by Yanshan Petrochemical Corp., Inc. China. The molecular weights obtained from GPC are $M_n = 9.6 \times 10^4$ g/mol and $M_w = 4.4 \times 10^5$ g/mol with a polydispersity $D = 4.6$.

2.2. Shear apparatus

A CSS 450 high-temperature shearing stage (Linkam Scientific Instruments Ltd., U.K.) was used to control the shear rate and thermal history of the iPP sample.

2.3. Rheo-optical microscopy

The rheo-optical study of the cylindrite structures was carried out with the use of a shear flow cell (CSS 450), which is connected to an optical microscope Nikon E600POL with video attachment. The iPP sample was melted at 200 °C for 5 min, then quenched to 140 °C and sheared for 5 s at a shear rate of 0.5 s^{-1}. After shear cessation, the iPP sample was isothermally crystallized at 140 °C and the shear-induced crystallization was recorded at different times. The shear time of 2 s was also applied to generate suitable cylindrite structure for measuring the length changes of the cylindrite core. The optical characteristic, i.e., the sign of birefringence of the micromorphologic feature was determined by means of a primary red filter (λ-plate) located diagonally between cross polarizers.

2.4. Rheo-light scattering

Time-resolved small-angle light scattering measurements were performed by home-constructed rheo-SALS, which was

adapted from Pogodina et al. [33] to allow the detection of polarization-dependent light scattering. Polarized light from a He–Ne laser (532 nm) was variably attenuated by a half-wave plate and a polarizing beam splitter. The polarized light was then steered to and focused on the scattering volume within a temperature-controlled, parallel quartz plate shear cell (CSS 450). The iPP sample was melted at 200 °C for 5 min, then quenched to 140 °C and sheared for 5 s at a shear rate of 0.5 s^{-1}. After shear cessation, the iPP sample was isothermally crystallized at 140 °C and the scattering patterns projected onto a semitransparent screen in the Hv and Vv polarization modes, respectively, were recorded with a two-dimensional CCD camera at different times. The schematic diagram of the optical setup and the coordinate system is shown in Fig. 1.

2.5. AFM

The shear-induced crystallized iPP sample at 140 °C for 2000 s was quenched to room temperature. The permanganic etching method initially developed by Bassett and Olley [60] and modified later [61] was applied to prepare the sample for AFM measurement. Etching was performed by shaking the sample in a 2% solution of potassium permanganate in a mixture (10 volume parts of concentrated sulphuric acid, 4 parts of orthophosphoric acid (85%), and 1 part of water) for 30 min. After etching, the sample was washed with distilled water, then dried in air for 24 h and further dried in vacuum at 50 °C for 48 h. The measurement was operated in the tapping mode with a NanoScope III MultiModeTM AFM (Digital Instruments), and both of the phase and height images were recorded simultaneously.

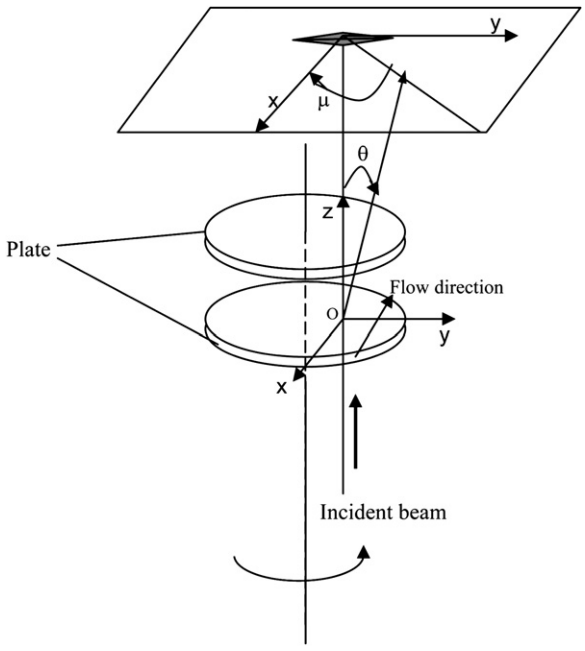

Fig. 1. Schematic diagram of the transparent plate–plate shear cell and the coordinate system for the experimental optical setup.

3. Results and discussion

3.1. Shear-induced crystallization of iPP by in situ optical microscopy

The shear-induced morphological development during crystallization was investigated by in situ optical microscope and the typical micrographs are shown in Fig. 2. It can be seen that after shear cessation, the thread-like textures are formed rapidly, which are actually shish-like core structures (see the micrograph at 10 s). At 140 s, the kebab-like structures are found to come into existence that are probably formed by a secondary nucleation of lamellae from the shish-like core surface in the transverse direction. As time prolonged, these kebab-like structures impinge with each other (at 540 s). At late stage, the quantity of newly formed crystals increases and these crystals impinge rapidly due to the space limit. Because of the perpendicular orientation of kebab-like structures to the shish core, finally the crystals (kebab-like structures) will grow and penetrate into spaces of other shish–kebab structures, and the shish-like core will be distracted and distorted, thus the overall orientation decreases as seen from the micrograph at 1940 s. These results are consistent with Hsiao's [62] experiment at high shear rate. In the following section, the corresponding SALS results in reciprocal space will be presented to verify the microscopic observation.

3.2. Time-resolved SALS measurement during shear-induced crystallization

Time-resolved SALS is particularly sensitive to density and orientation fluctuations at micron scale in the early stages of polymer crystallization. The classical theory of SALS [63–68] allows quantitative interpretation of quiescent crystallization. However, this theory is not suitable for the oriented crystalline structures in the polarization-dependent SALS measurements. Here, we followed the Hashimoto's method [69,70] to quantitatively investigate the polarization-dependent SALS results with two polarization modes Vv and Hv during the shear-induced crystallization of iPP.

The light scattering intensity $I(q_x, q_y)$ was measured in the plane O_{xy}, where q_x and q_y are the x and y components of the scattering vector $\boldsymbol{q}$ (i.e. $\mu = 0$ and 90° in Fig. 1, respectively). The magnitude of q is related to the scattering angle, θ and the wavelength, λ as follows:

$$q = (4\pi/\lambda)\sin(\theta/2) \tag{1}$$

The shear-induced crystallization can be analyzed by measuring the integrated scattering intensities, $Q_{\parallel}(t)$ and $Q_{\perp}(t)$, parallel and perpendicular to the flow direction, respectively, as functions of crystallization time, t. $Q_{\parallel}(t)$ and $Q_{\perp}(t)$ are defined by the following equations:

$$Q_{\parallel}(t) = \int_{q_{\min}}^{q_{\max}} \mathrm{d}q_y I(q_x, q_y) \tag{2}$$

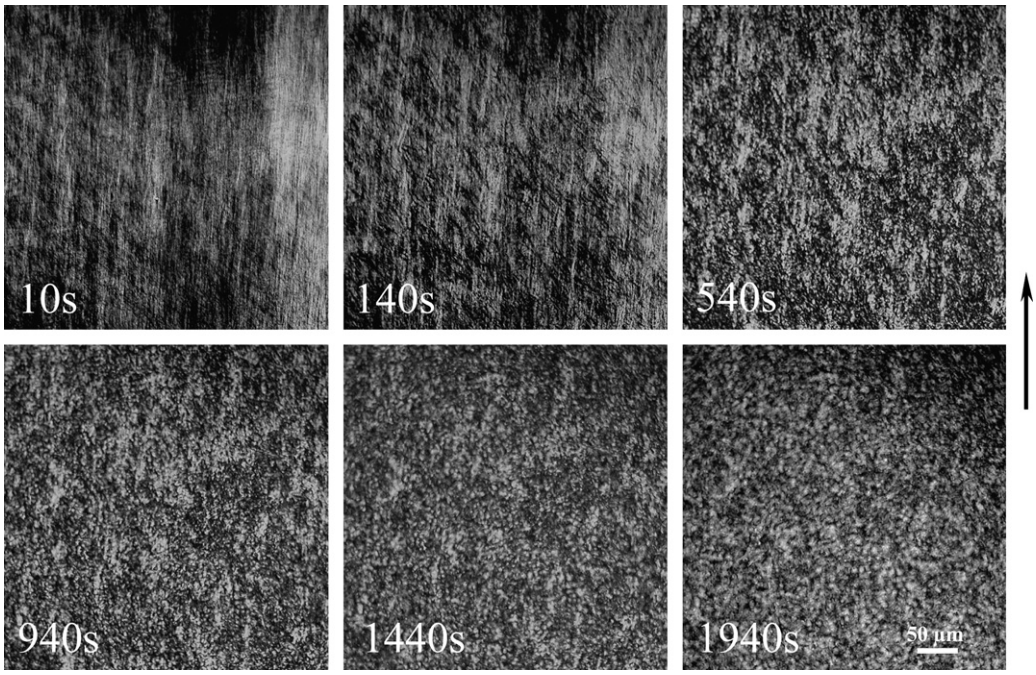

Fig. 2. In situ micrographs of iPP during shear-induced crystallization. iPP was melted at 200 °C for 5 min, then quenched to 140 °C and sheared for 5 s at a shear rate of 0.5 s^{-1}. After shear cessation, the sample was isothermally crystallized at 140 °C. The black arrow indicates the flow direction.

$$Q_{\perp}(t) = \int_{q_{\min}}^{q_{\max}} \mathrm{d}q_x I(q_x, q_y) \tag{3}$$

Here $q_{\min}$ and $q_{\max}$ are the experimental limits in the SALS setup.

The time-resolved SALS patterns in Vv and Hv modes during the shear-induced crystallization of iPP are shown in Fig. 3, respectively. The SALS streaks are oriented perpendicular to the flow direction. From Fig. 3 it can be seen that the streaks are more pronounced in Vv mode than in Hv mode at the early stages of crystallization. Appearance of the streaks indicates the immediate formation of shish-like core after shear. Much stronger streaks in the direction perpendicular than parallel to the shear direction indicate that the crystallized structures are highly anisotropic. Preferential orientation of the streaks perpendicular to the shear direction is the consequence of the elongated structures (shish-like core) formed due to the shear flow. The scattering intensity in the flow direction increases with the crystallization time, which indicates that kebab-like structures grow with time. At the late stages of crystallization, the scattering patterns become more isotropic. This infers that the shish–kebab-like structures impinge into each other and finally the lamellae (kebabs) grow and penetrate into spaces of other shish–kebab structures, leading to the disappearance of the anisotropy.

The anisotropic SALS patterns shown in Fig. 3 are typical for the shear-induced crystallization of iPP in our experiment. This result is consistent with that of Pogodina et al. [33]. Fig. 4 shows the double-logarithmic plots of the normalized integrated scattering intensities parallel and perpendicular to the flow direction, $Q_{\parallel}(t)/Q_{\parallel}(t=0)$ and $Q_{\perp}(t)/Q_{\perp}(t=0)$ as functions of crystallization time after shear cessation. The results in Vv and Hv modes in Fig. 4 show the similar tendency, that is, after shear cessation, the integrated intensity perpendicular to the flow direction quickly increases with time, which indicates the immediate formation of shish-like structures after shear. Then, the normalized integrated intensity reaches the maximum. At such low shear rate shish-like structure is probably formed by bundles of the entangled network chains. After some of the network chains are being stretched and form anisotropic bundles, some crystal might be quickly developed with the nucleus of these bundles and the integrated intensity reaches the maximum. The integrated intensity parallel to the flow direction also increases with time, but some time later reaches to the close maximum values as that perpendicular to flow direction. According to the optical microscopic observation, shish-like structures grow parallel to the flow direction, while kebab-like structures grow perpendicular to the flow direction. In reciprocal space, the results of SALS are consistent with that in real space. In Fig. 3, at the early stage of crystallization, the scattered intensity parallel to the flow direction is very weak, which indicates that kebab-like structures may not form, while the strong scattered intensity perpendicular to the flow direction infers that shish-like structure forms immediately after shear cessation. Thus, at the early stage of crystallization the integrated intensity perpendicular to the flow direction is stronger than that parallel to the flow direction. At the late stage, kebab-like structures impinge into each other, and the integrated intensity parallel to the flow direction cannot increase continuously. Finally, the crystals (kebab-like structures) might grow and penetrate into spaces of other shish–kebab structures, and many crystals occupy the shish space, therefore, the integrated intensity parallel to the flow direction reaches to the

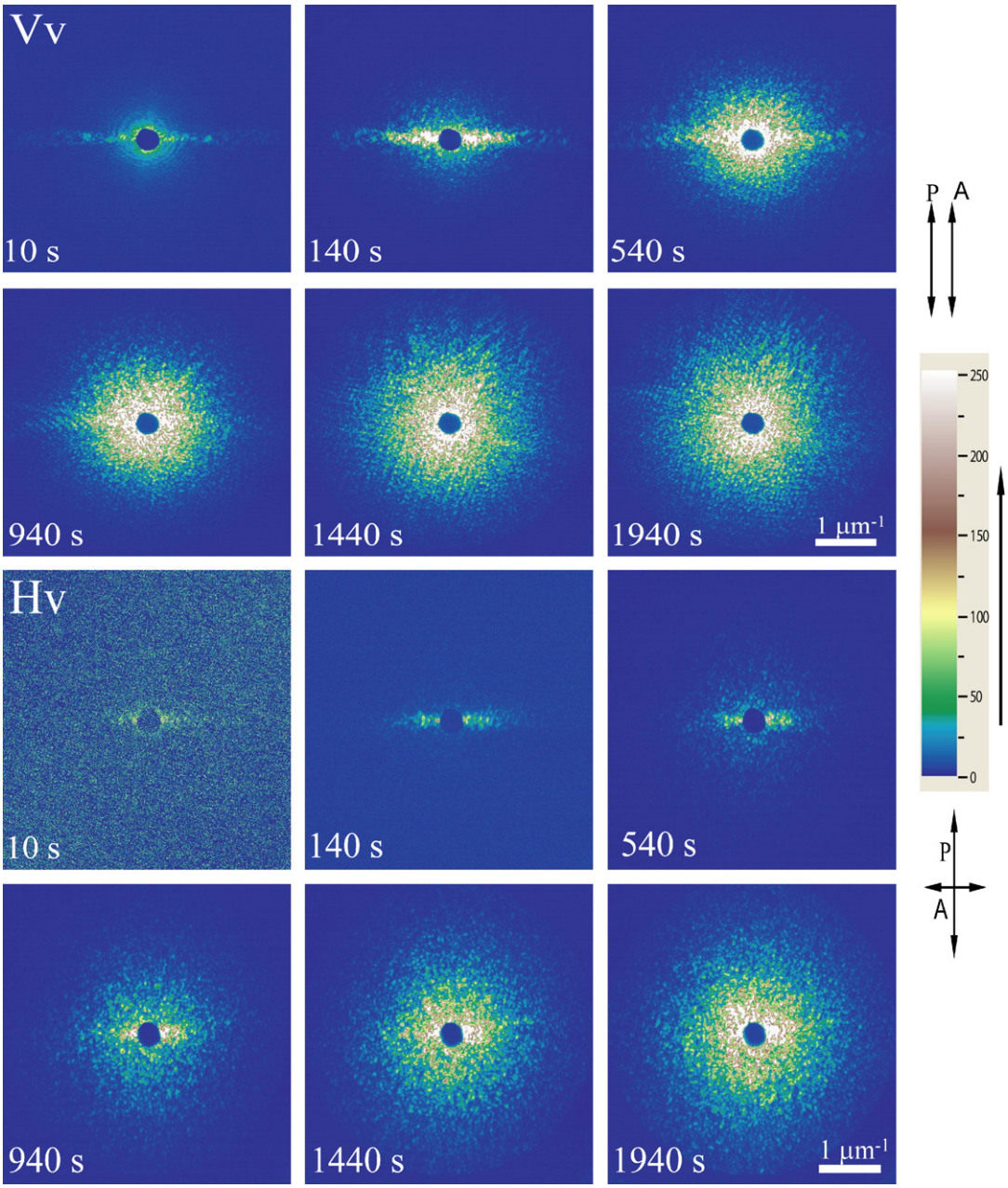

Fig. 3. In situ SALS patterns during shear-induced crystallization of iPP in Vv and Hv modes. iPP was melted at 200 °C for 5 min, then quenched to 140 °C and sheared for 5 s at the shear rate of 0.5 s^{-1}. The single-end arrow indicates the flow direction.

maximum, and the SALS patterns become isotropic. It is noted that we have obtained similar results at different shear rates, suggesting that the above phenomena are quite universal for the system we have studied.

3.3. Length changes of the shish-like core during isothermal crystallization

It is generally accepted that during the development of the cylindrite structures, the cylindrical structure grows larger, and kebab-like structures become longer and longer, assuming that the shish-like structure grows with time in the same way as the kebab-like structures grow under the same condition. Hsiao et al. [21–23] have estimated the shish-like structure length by employing the Ruland method from the SAXS data. They found that the shish-like structure shrinks or its average length decreases instead of increasing with time after shear cessation. They gave reasons for the shish-like structure shrinking as follows: (i) the relaxation of chain ends and loss of the average degree of orientation after the shear cessation, (ii) the development of kebab-like structures imposing a local stress at several discrete points along the shish-like structure and relaxing its orientation with respect to the flow direction, and (iii) the formation of a shorter shish–kebab-like structure from the less stretched chains at the later time.

The shish-like structure growth from iPP melt observed in the real space by optical microscopy is displayed in Fig. 5. The length of the shish-like structure located in the middle

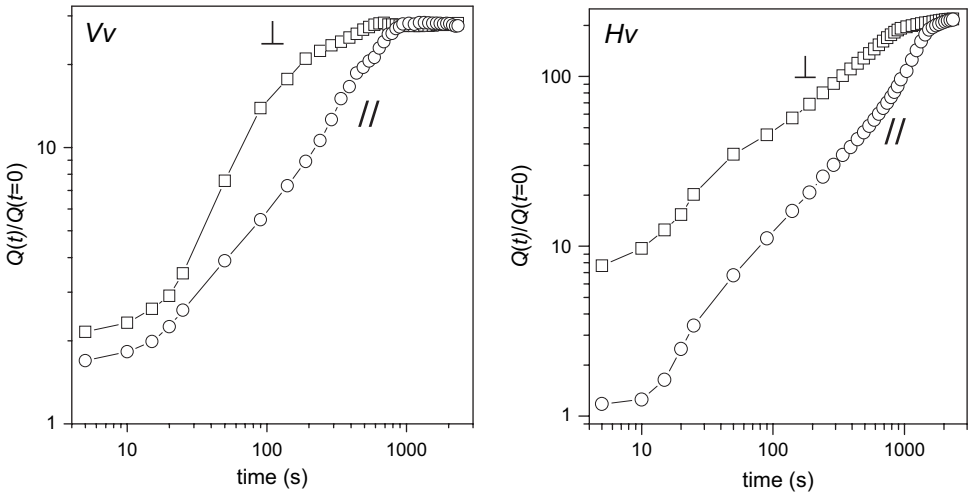

Fig. 4. Plots of normalized $Q_{\parallel}(t)/Q_{\parallel}(t=0)$ and $Q_{\perp}(t)/Q_{\perp}(t=0)$ as functions of crystallization time in Vv and Hv modes, respectively.

in each micrograph is tabulated in Table 1. It is seen that the length of shish-like structure does not change or changed very little during crystallization. However, Hsiao's results showed that the shish-like structure length shrank about 30–50%. We believe that the difference is related to the different experimental conditions. First of all, the effect of molecular weight is minor between these two studies. In Hsiao's experiment the molecular weights of iPP are $M_n = 9.2 \times 10^4$ g/mol and $M_w = 3.68 \times 10^5$ g/mol, which are similar to the iPP sample in our present work. So, molecular weight is not the reason. Second, the experimental temperature of 165 °C from Hsiao's reports is close to the nominal melting point of iPP. It is well known that crystallization and melting are a pair of competing dynamic processes. When the temperature is close to the nominal melting point, the polymer crystallization becomes difficult because of the slow nucleation. Meanwhile, the crystallized chains can be melted and diffused into the melts with less energy barrier. Thus, the crystallization process is mainly controlled by nucleation at high temperature. Long induction period is needed for the kebab-like structures to form induced from the shish-like core. The nuclei of the shish–kebab-like structure (the shish part) could possibly relax into the amorphous state, leading to the shish-like core shrinking. When the crystallization occurs at a much low temperature that is our case, the shish shrinking should be much less. Third, the shear strain may affect the length of shish. The higher the shear rate and shear strain, the easier the breaking-up or distorting of the shish–kebab-like structure and the decreasing of the shish-like core. To summarize, Hsiao et al. observed the longer shish-like core after shear cessation, and the shish-like core became shorter, caused by chain relaxation with crystallization time. While in our case, the crystallization temperature is much lower, and relaxation of the oriented chains must overcome higher energy barrier, therefore the shish-like core can preserve its length

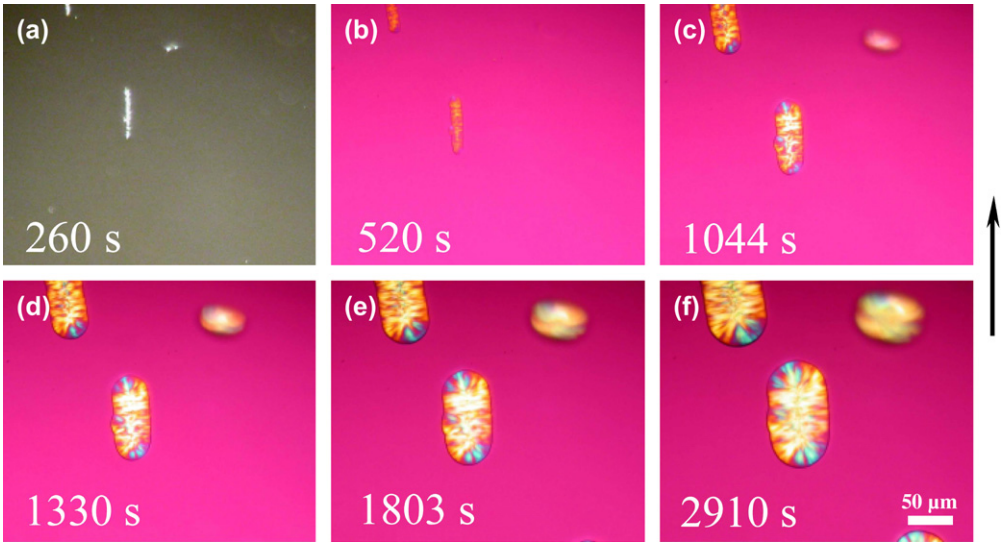

Fig. 5. Optical micrographs of the shish-like structure growth from iPP melt. iPP was melted at 200 °C for 5 min, then quenched to 140 °C and sheared for 2 s at a shear rate of 0.5 s^{-1}. After shear cessation, the sample was isothermally crystallized at 140 °C for different times. The arrow indicates the flow direction.

Table 1
Length of the shish-like structure in Fig. 5 at different crystallization times

Time (s)	260	520	1044	1330	1803	2910
Length (μm)	82	81	82	81	82	82

during crystallization. Therefore, we believe the difference is explainable.

3.4. Aligned spherulites in shear-induced crystallized iPP after quenching

According to our previous work [53], the shear-induced crystallization of iPP exhibits perfect cylindrite structure at 140 °C parallel to the shear direction. When the sample was quenched to room temperature, large spherulites grew over the cylindrite structure and eventually cover the cylindrite structure. If the quenched shear-induced crystallized iPP sample has not been etched, the cylindrite structures are difficult to be observed by AFM [27]. Fig. 6 shows the optical micrographs of the quenched shear-induced iPP crystal samples after etching. It can be seen in the polarized microscopy that there are spherulites well aligned in the vicinity of the cylindrite structure, where the cylindrite structure cannot be clearly observed (Fig. 6a). However, the cylindrite structure can be distinctly observed in the bright field (Fig. 6b).

3.5. Cylindrite morphology observed by AFM

Fig. 7 shows typical phase images of the shear-induced crystallized iPP sample for 2000 s after quenching to room temperature. These images exhibit a long shish in the core and the kebabs along the shish, which are similar to those in the in situ microscopic observation. The shish-like structure of the cylindrite can be observed clearly. We can distinguish the lamellae of kebab-like structures grown from the central shish core (Fig. 7b). The lamellae of the kebab-like structure are covered with the amorphous phase (the arrows indicate the amorphous phase). However, the detailed lamellae of the cylindrite structures cannot be clearly observed due to the covering of the amorphous phase and the newly formed crystals during further quench of the sample to the room temperature.

In order to study the cylindrite structure, the shear-induced crystallized iPP sample was etched by potassium permanganate solution of concentrated sulphuric acid and orthophosphoric acid. Fig. 8 shows the height and phase images of the etched sample. From the height image (Fig. 8a), a high ridge (pointed out by arrow 1) is seen, which represents the shish-like structures. The lamellae (by arrow 2) adjacent to the ridge form kebab-like structures. From the phase image, the average ridge width is about 1–2 μm. Compared with Fig. 7, because the amorphous phase was etched, the ridge in Fig. 8 should be

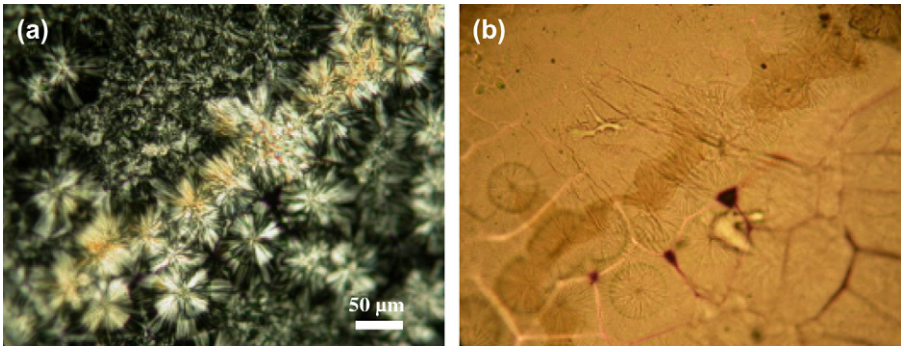

Fig. 6. Optical micrographs of the shear-induced crystallized iPP after quenching to room temperature. The sample was etched for 0.5 h by 2% potassium permanganate solution of concentrated sulphuric acid and orthophosphoric acid. The shear condition is the same as in Fig. 2. (a) Polarized field; (b) bright field.

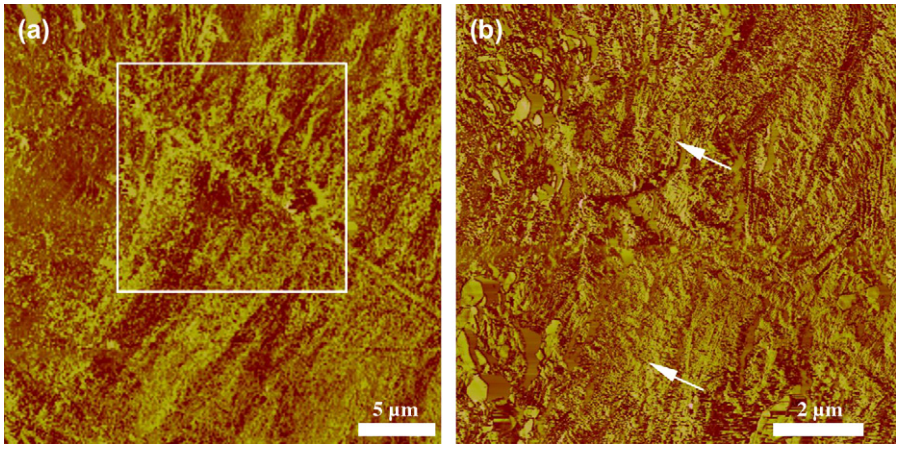

Fig. 7. Phase images of the shear-induced crystallized iPP sample by AFM to demonstrate the cylindrite structure. Right image corresponds to the part in the white box of the left image.

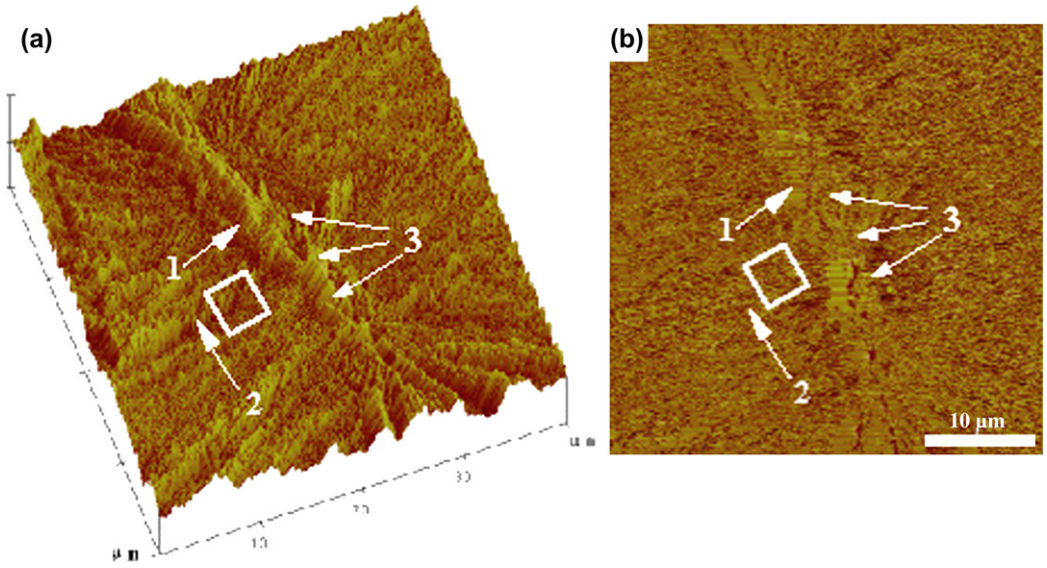

Fig. 8. Height (a) and phase (b) images of the shear-induced crystallized iPP sample by AFM. The sample was etched for 0.5 h by 2% potassium permanganate solution of concentrated sulphuric acid and orthophosphoric acid. The white box is the section of Fig. 9.

the crystalline phase. The important question is how the ridge or the shish-like structure has been developed. Compared with the radius of gyration of a molecule (~20–30 nm), the width of the "shish" (1–2 μm) is much larger. Obviously, the number of molecules involved in such process of forming shish–kebab-like cylindrite structure at low shear rate and low temperature is very large. We know that polymer chains at high enough molecular weight entangle and form network structure in melt. At low temperature, the entangled polymer network structure is difficult to disentangle under shear due to the long relaxation time and the existence of helical segments [53]. The applied stress can be distributed over a long distance (relative to the single molecular chain length) due to entangled network structure. The entangled polymer network structure may be deformed, and the bundle of strands between entanglement points may form anisotropic structures. These bundles of strands are oriented along the flow direction, and developed into the nuclei (shish-like structure) at the early stage of crystallization. At the late stage of crystallization, the ridge has become wide. The fully stretched polymer chain cannot be clearly observed by AFM. However, the stretched chain bundles exist and form the extended crystals, and then become the row nuclei and induce the shish–kebab-like structure. In our work, shish-like structure of the extended crystals could not be observed, instead shish-like structure from the chain bundles with defects (by arrow 3) along the "shish" direction was observed, which could come from the trapped entanglement junctions as shown in Fig. 8.

Fig. 9 shows the fine kebab-like structure of shear-induced crystallization. This is actually a section on the side of Fig. 8 (white box). By using the retrace phase signals along the lamellae, the average distance between two kebab-like structures was estimated to be 60–80 nm (Fig. 9a), which is similar to Hobbs' observation [52]. The average thickness of

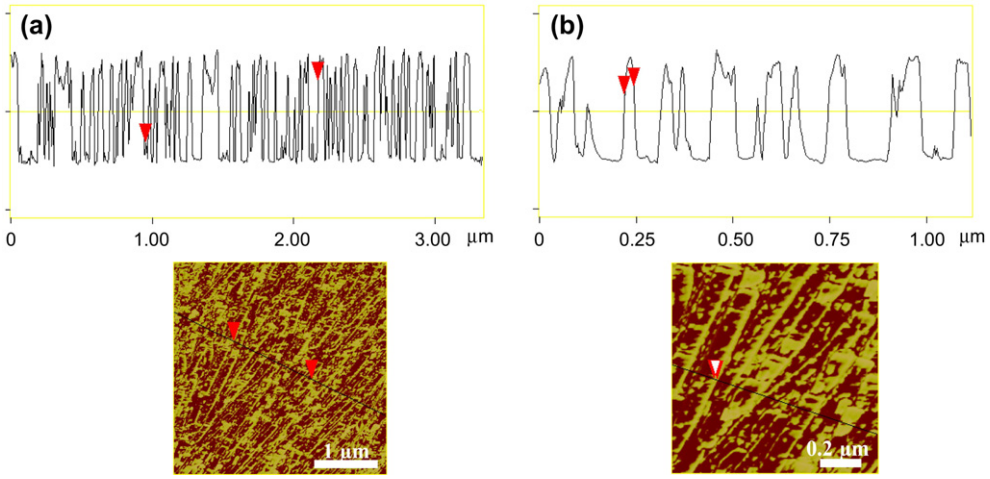

Fig. 9. Measurements of the distance between two kebabs (a) and the lamellar thickness (b).

the lamellae was measured to be approximately 20–30 nm (Fig. 9b). It is noted that the values could be affected by the tip–surface convolution effect when the tip size (~20 nm) is similar to that of the measured objects [71]. Considering the lamellar thickness and the surrounding melt, any newly formed nuclei in-between the lamellae may not grow to sufficient sizes to survive. In other words, the 60–80 nm distance between the kebab-like structures may not be large enough to accommodate new lamellae, even though the thickness could be less than 30 nm. Usually, there are amorphous phases on each side of the lamella, so the distance between the next-nearest neighbors is ~100 nm.

3.6. Analysis of shish–kebab-like cylindrite morphology with shear

Polymer chains entangle in concentrated solutions or melts. Entanglement implies that two chains are tightly kinked around each other by bending back themselves in short-range contour. According to Bueche theory [72], the average molecular weight spacing between entanglement points is "M_e". The entanglement in polymer melt is only a topological "knot" which only becomes a tight knot during shear or with the possible existence of a helical segment formed knot. When the temperature is close to the nominal melting points, polymer chains are easy to move due to the high kinetic energy, and entanglement points tend to disentangle under shear. In contrast, the disentanglement of polymer chains at lower temperature is more difficult. At low temperature, the entangled network can be deformed and oriented along the shear direction. At low shear rate, only certain section of polymer chains can be extended while the remaining section stays in the random conformation.

After shear cessation, the scattering streak was immediately observed in reciprocal space. That implies that the shish-like structure formed first, and was followed by kebab-like structures. The scattering intensity rapidly increased within a short time, which indicates that bundles in the shish-like structure significantly induce the amorphous coiled chains to crystallize. In Figs. 7 and 8, the width of shish-like core was 1–2 μm. However, in Hsiao's reports [23,27], the width of shish was much smaller and the average diameter of the outer kebabs approaches 0.3–0.4 μm. We suggest that in our experiment the shish-like structure is formed from the bundles of entangled network at low shear rate; otherwise, the shish-like structure observed in our experiment should have similar width to or a little wider than Hsiao's observation. Hsiao et al. did the experiments at high temperature and high shear rate. At high temperature, polymer chains are easier to move, and entanglement tends to disentangle at high shear rate. Therefore, we think that the formation mechanisms of shish–kebab-like cylindrite structure could be somehow different between that at high temperature with high shear rate and that at low temperature with low shear rate. In addition, the relaxation of deformed entanglement network may take longer time than that of the stretched single chains. Thus, if the shish-like structure is formed from the entangled network, the length of shish core should not change obviously. Because the stretched single chains can relax much easier, shortening of shish core could be observed in Hsiao's experiment at high temperature and high shear rate.

3.7. Mechanism of shish–kebab-like cylindrite formation at low temperature and low shear rate

From AFM results, the fully stretched chains along the shish cannot be observed within the resolution limitation. It may be proper to state that the coil–stretch transition happens at high shear rate (such as shear rate = 100 s^{-1} for a typical Newtonian to non-Newtonian transition). For the low shear rate, an alternative mechanism for forming the shish–kebab-like cylindrite structure has been proposed in our previous work [53]. In this mechanism, the shish-like structure is a bundle of shear-stretched strands, which forms the nuclei to induce the growth of the kebabs.

Based on our study in this work, we speculate that the mechanism of shear-induced crystallization at low temperature and low shear rate may be different from that at high temperature and high shear rate. Our proposed mechanism is illustrated in Fig. 10. First of all, the schematic of partial orientation of entangled polymer chains in melt at low shear rate is shown in Fig. 10A. The entangled polymer networks are distorted under shear and form the aligned bundle of strands between entanglement points. Fig. 10B shows the mechanism of shear-induced crystallization at low temperature and low shear rate. It is well known that crystallization under shear is a multi-step sequential process. When shear flow was imposed on polymer melt, polymer chains may be stretched and oriented along flow direction, especially at low temperature, and some helical segments may be formed at the entangled junctions. At low shear rate, single chains may not be stretched and developed into the extended chain bundles. Instead, there are some sections of network chains that can be partially disentangled and stretched through the entangled network junctions and then form the fibrillar crystals and finally developed into the shish. The shish-like structure can serve as nucleation sites for the tangential growth of the kebabs. The normal of the lamellae of the kebab-like structures is parallel to flow direction. At the late stages of crystallization, the chain-folded lamellae with the spherulitic morphology may form in the amorphous phase. In the literature [27], the formation mechanism of the shish–kebab is similar to ours, however, they thought that the high molecular weight materials are important to form net structure. In our proposed mechanism, we think that entanglement molecular weight M_e is important to form this structure. The high molecular weight fraction may be helpful and make this process easier. Throughout this article, we have used the terms "shish–kebab", "shish–kebab-like cylindrite" and "cylindrite", just because we could not think a better way to describe the structures formed in our experiments and make a comparison with other studies. We believe that the cylindrite structure formed at low temperature and low shear rate is definitely different from the ones from solution under shear. It may even

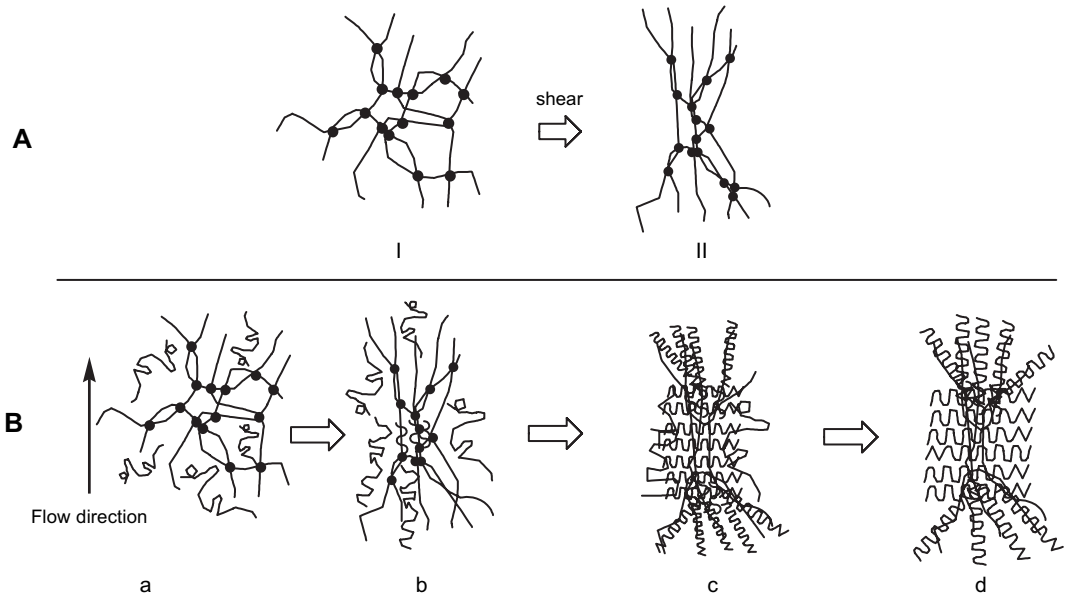

Fig. 10. (A) Illustration of partial oriented polymer chains in melt at low shear rate. (I) Amorphous melt; (II) entangled network which becomes distorted under shear. (B) Schematic of shish–kebab formation under shear: (a) entangled network in melt; (b) shear-induced row nuclei were grown from the stretched and aligned bundles of strands between entanglement points; (c) epitaxial growth of shish–kebab-like cylindrite; (d) final shish–kebab-like cylindrite. Black dots indicate the entanglement points.

be different from those formed in melt at high temperature and high shear rate.

4. Conclusions

The shear-induced crystallization of iPP at low temperature and low shear rate was investigated by in situ optical microscope, time-resolved SALS, and ex situ AFM. The results of optical microscopic observation indicate that the shish-like structures are formed rapidly after shear cessation. At late stage, the quantity of newly formed crystals increases and these crystals impinge into each other rapidly due to the space limitation. Measurement of shish core length from optical microscopic observation showed that the shish core length either did not change or changed very slightly during crystallization. SALS results confirmed the formation of shish–kebab-like cylindrite structures in iPP at the low shear rate. A highly oriented structure emerged at first to produce the scattering streak perpendicular to the flow direction, and then the scattered intensity rapidly increased with crystallization time. Eventually, the scattered intensity became circularly symmetric and the anisotropy decreased significantly. By the analysis of the AFM images of the etched iPP samples, a much wider shish-like structure was observed. Compared with the radius of gyration of a molecule, the process of shear-induced crystallization may have involved a large number of molecules under low shear rate. Therefore, we believe that the shear-induced cylindrite formation of polymer melt at low temperature and low shear rate must have started from the stretching and orienting of the entangled network strands. According to this study, the formation mechanism of shish–kebab during shear-induced crystallization at low temperature and low shear rate can be described as follows: when shear flow is imposed on polymer melt, polymer chain strands may be stretched and oriented along flow direction, and some sections of the entangled network chains are partially disentangled and stretched through the entangled network junctions and then formed the fibrillar crystals, which in turn developed into the shish, and finally the kebabs grew with their normal parallel to the flow direction.

Acknowledgements

We acknowledge financial supports from the National Science Foundation of China (NSFC, Grant Nos. 20490220, 20574081 and 10590355), Directional Innovation Project of CAS (KJCX2-SWH107), and 973 Program of MOST of China (2003 CB 615600). Z.G. Wang acknowledges financial support from ‘Hundred Young Talents’ Program of CAS and the National Science Foundation of China.

References

[1] Pennings AJ, Kiel AM. Kolloid Z Z Polym 1965;205:160.
[2] Pennings AJ, Van der mark JMA, Booij HC. Kolloid Z Z Polym 1970; 236:99.
[3] Petermann J, Miles M, Gleiter H. J Polym Sci Part B Polym Phys 1979; 17:55.
[4] Varga J. J Mater Sci 1992;27:2557.
[5] Varga J, Karger-Kocsis J. J Polym Sci Part B Polym Phys 1996;34:657.
[6] Lieberwirth I, Loos J, Petermann J, Keller A. J Polym Sci Part B Polym Phys 2000;38:1183.
[7] Bove L, Nobile MR. Macromol Symp 2002;185:135.
[8] Lellinger D, Floudas G, Alig I. Polymer 2003;44:5759.
[9] Watanabe K, Suzuki T, Masubuchi Y, Taniguchi T, Takimoto J, Koyama K. Polymer 2003;44:5843.
[10] Ran S, Wang Z, Burger C, Chu B, Hsiao BS. Macromolecules 2002;35: 10102.

[11] Wu CM, Chen M, Karger-Kocsis J. Polymer 1999;40:4195.
[12] Keller A, Kolnaar HW. Mater Sci Technol 1997;18:189.
[13] Keller A, Hikosaka M, Rastogi S, Toda A, Barham PJ, Goldbeck-Wood G. J Mater Sci 1994;29:2579.
[14] Keller A, Cheng SZD. Polymer 1998;39:4461.
[15] Mackley MR, Keller A. Polymer 1973;14:16.
[16] Pope DP, Keller A. Colloid Polym Sci 1978;256:751.
[17] Miles MJ, Keller A. Polymer 1980;21:1295.
[18] Somani RH, Hsiao BS, Nogales A, Srinivas S, Tsou AH, Sics I, et al. Macromolecules 2000;33:9385.
[19] Fu BX, Yang L, Somani RH, Zong SX, Hsiao BS, Phillips S, et al. J Polym Sci Part B Polym Phys 2001;39:2727.
[20] Somani RH, Hsiao BS, Nogales A, Srinivas S, Tsou AH, Balta-Calleja FJ, et al. Macromolecules 2001;34:5902.
[21] Yang L, Somani RH, Sics I, Hsiao BS, Kolb R, Lohse D, et al. Macromolecules 2004;37:4845.
[22] Somani RH, Yang L, Hsiao BS, Sun T, Pogodina NV, Lustiger A. Macromolecules 2005;38:1244.
[23] Hsiao BS, Yang L, Somani RH, Avila-Orta CA, Zhu L. Phys Rev Lett 2005;94:117802.
[24] Somani RH, Yang L, Hsiao BS, Agarwal P, Fruitwala H, Tsou AH. Macromolecules 2002;35:9096.
[25] Agarwal P, Somani RH, Weng W, Mehta A, Yang L, Ran S, et al. Macromolecules 2003;36:5226.
[26] Somani RH, Yang L, Hsiao BS. Physica A 2002;304:145.
[27] Somani RH, Yang L, Zhu L, Hsiao BS. Polymer 2005;46:8587.
[28] Ran S, Zong X, Fang D, Hsiao BS, Chu B, Phillips RA. Macromolecules 2001;34:2569.
[29] Nogales A, Hsiao BS, Somani RH, Srinivas S, Tsou AH, Balta-Calleja F, et al. Polymer 2000;42:5247.
[30] Eder G, Janeschitz-Kriegl H. Mater Sci Technol 1997;18:268.
[31] Jerschow P, Janeschitz-Kriegl H. Int Polym Proc 1997;12(1):72.
[32] Eder G, Janeschitz-Kriegl H, Liedauer S. Prog Polym Sci 1990;15:629.
[33] Pogodina NV, Lavrenko VP, Winter HH, Srinivas S. Polymer 2001;42:9031.
[34] Pogodina NV, Siddiquee SK, Egmond JW, Winter HH. Macromolecules 1999;32:1167.
[35] Pogodina NV, Winter HH, Srinivas S. J Polym Sci Part B Polym Phys 1999;37:3512.
[36] Pogodina NV, Winter HH. Macromolecules 1998;31:8164.
[37] Li L, Jeu WH. Phys Rev Lett 2004;92:075506.
[38] Li L, Jeu WH. Macromolecules 2003;36:4862.
[39] Duplay C, Monasse B, Haudin J, Costa J. Polym Int 1999;48:320.
[40] Haudin J, Duplay C, Monasse B, Costa JL. Macromol Symp 2002;185:119.
[41] Monasse B. J Mater Sci 1995;30:5002.
[42] Jay F, Haudin JM, Monasse B. J Mater Sci 1999;34:2089.
[43] Duplay D, Monasse B, Haudin J, Costa J. J Mater Sci 2000;35:6093.
[44] Liu C, Muthukumar M. J Chem Phys 1998;109:2536.
[45] Muthukumar M, Welch P. Polymer 2000;41:8833.
[46] Dukovski I, Muthukumar M. J Chem Phys 2003;118:6648.
[47] Hu W, Frenkel D, Mathot VBF. Macromolecules 2002;35:7172.
[48] Ryan AJ, Stanford JL, Bras W, Nye TMW. Polymer 1997;38:759.
[49] Coppola S, Grizzuti N, Maffettone PL. Macromolecules 2001;34:5030.
[50] Okamoto M, Kubo H, Kotaka T. Macromolecules 1998;31:4223.
[51] Pople JA, Mitchell GR, Sutton SJ, Vaughan AS, Chai CK. Polymer 1999;40:2769.
[52] Hobbs JK, Miles MJ. Macromolecules 2001;34:353.
[53] Zhang C, Hu H, Wang D, Yan S, Han CC. Polymer 2005;46:8157.
[54] de Gennes PG. J Phys Chem 1974;60:5030.
[55] Pennings J, Pijpers MFJ. Macromolecules 1970;3:261.
[56] Smith DE, Babcock HP, Chu S. Science 1998;281:1335.
[57] Smith DE, Babcock HP, Chu S. Science 1999;283:1724.
[58] Abuzaina FM, Fitz BD, Andjelic S, Jamiolkowski D. Polymer 2002;43:4699.
[59] Kumaraswamy G, Issaian AM, Kornfield JA. Macromolecules 1999;32:7537.
[60] Bassett DC, Olley RH. Polymer 1982;23:1707.
[61] Shahin MM, Olley RH, Blissett MJ. J Polym Sci Part B Polym Phys 1999;37:2279.
[62] Somani RH, Yang L, Sics I, Hsiao BS, Pogodina NV, Winter HH. Macromol Symp 2002;185:105.
[63] Stein RS, Wilson PR. J Appl Phys 1962;33:1914.
[64] Debye P, Anderson HR, Brumberger H. J Appl Phys 1957;28:679.
[65] Debye P, Bueche AM. J Appl Phys 1949;20:518.
[66] Koberstein J, Russell TP, Stein RS. J Polym Sci Part B Polym Phys 1979;17:1719.
[67] Yoon DY, Stein RS. J Polym Sci 1974;12:735.
[68] Stein RS, Rhodes MB. J Appl Phys 1960;31:1873.
[69] Murase H, Kume T, Hashimoto T, Ohta Y, Mizukami T. Macromolecules 1995;28:7724.
[70] Kume T, Hashimoto T, Takahashi T, Fuller GG. Macromolecules 1997;30:7232.
[71] Trifonova D, Varga J, Vancso GJ. Polym Bull 1998;41:341.
[72] Bueche F. Physical properties of polymers. New York: Interscience; 1962.